Organic & Biomolecular Chemistry

Accepted Manuscript

ROYAL SOCIETY OF CHEMISTRY

www.rsc.org/obc

INTRODUCTION

The amidic derivative of 4-amino-TEMPO (*N*-acetylamino-2,2,6,6-tetramethylpiperidine-*N*-oxide, AA-TEMPO, Figure 1) has been recently identified as a promising oxidation catalyst.[1] This stable nitroxide is currently produced on industrial scale as an emerging substitution for widely used radical oxidant TEMPO[2,3] (Figure 1).

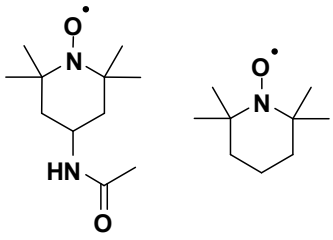

AA-TEMPO TEMPO

Figure 1. Nitroxide-type oxidation catalysts.

Despite the lack of π-conjugation in their saturated skeletons, various TEMPO derivatives show a clear dependence of their physicochemical properties (stemming from the presence of a radical site) on the electronic nature of C-4 substituents.[4,5] The deeper insight into these effects is crucial for the rational design and practical utilisation of stable nitroxides[6] as perspective functional materials including radical batteries,[7] magneto-active compounds,[8] redox mediators in dye-sensitised solar cells,[9] and/or multi-responsive copolymers.[10] Moreover, there are an emerging medicinal applications of low-toxic nitroxides as fMRI contrast enhancing[11] and radiation protective agents,[12] topical drugs for alopecia prevention,[13] and/or antioxidants displaying antihypertensive effects.[14] Within this broad context, we are interested in the targeted design, practical synthesis and properties evaluation of novel mono/dinitroxyl amides inspired by AA-TEMPO. Thus, we have designed and prepared series of novel mononitroxyl amides/carbamate **4**–**9** and dinitroxyl amides/ureas **10**–**13** as two comparative sets and systematically investigated the influence

of (stereo)electronic effects of *N*-substituents and/or nitroxide's ring size on the spectroscopic properties, electrochemical behaviour as well as potentially useful biological activity of studied compounds.

RESULTS AND DISCUSSION

Synthesis. While starting mononitroxides 4-amino-TEMPO **1** and 3-amino-PROXYL **2** are commercially available, the known dinitroxide **3** was readily prepared *via* modified[5] synthetic protocol.[15] All three starting radicals **1**–**3** (Figure 2) are sufficiently stable under standard storage conditions and do not readily decompose even at slightly elevated temperature.[16]

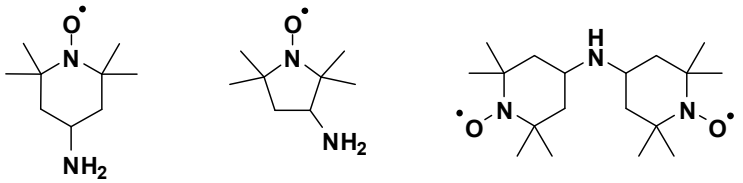

Figure 2. Starting aminonitroxides **1**–**3**.

Thus, employing **1** and **2** as substrates, we have designed and prepared a set of *N*-substituted TEMPO **4**–**8** and PROXYL **9** monoradicals. For comparison purposes, we have chosen bulky pivaloyl amide **4**[17] and carbamate **5**,[18] electron-donating benzamide **6** and formamide **7**,[19] and electron-withdrawing trifluoroacetamides **8**[20] and **9**. The synthesis of all mononitroxides consisted of standard one-step *N*-carbonylations with either chlorides, anhydrides and/or formate as corresponding electrophiles. The desired amidic derivatives **4**–**9** were obtained in high purity and good to excellent yields (72-93%) after FLC (Scheme 1).

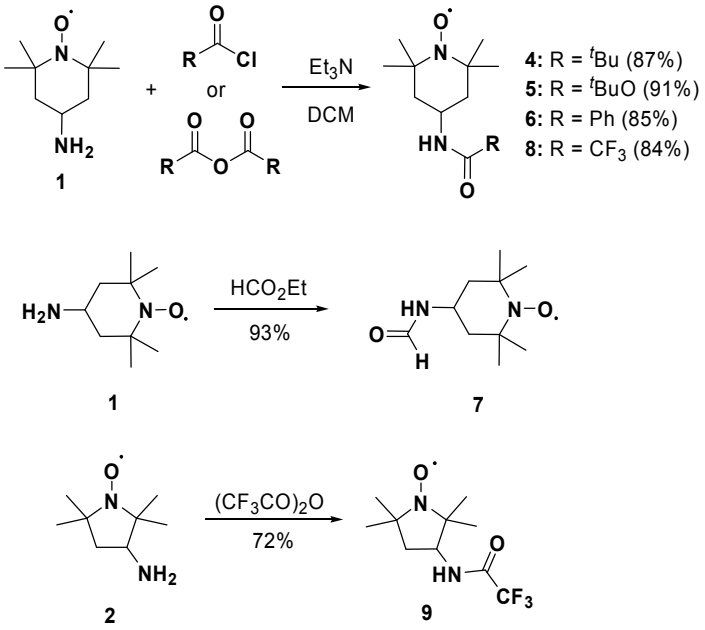

Scheme 1. Synthesis of mononitroxides **4**–**9**.

In order to compare the properties of amidic mono- *vs.* biradicals, we have envisaged tertiary amides **10** and **11**. Analogously to the abovementioned mononitroxides, biradicals **10** and **11** were prepared from *bis*-TEMPO-amine **3** by its carbonylations with corresponding anhydrides in the presence of triethylamine in good to moderate yields (81% resp. 69%, Scheme 2).

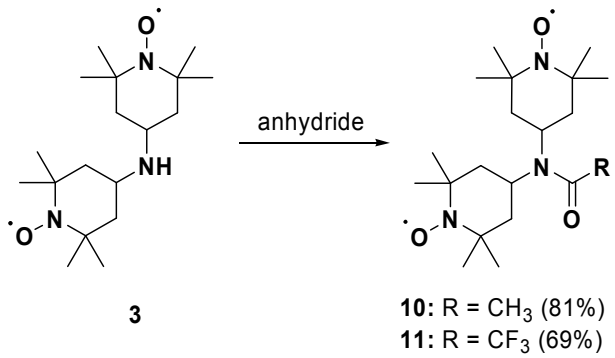

Scheme 2. Synthesis of dinitroxides **10** and **11**.

Finally, to examine the influence of 6- *vs.* 5-membered ring on the physicochemical properties of dinitroxides, we have prepared *bis*-TEMPO and *bis*-PROXYL ureas **12** and **13**. While the original carbonylative conditions[21] (Boc_2O, DMAP, MeCN) provided a desired derivative **12** in 23% yield only, our modified synthetic protocol involving 1,1'-carbonyldiimidazol (CDI) as a coupling reagent furnished both ureas **12** and **13** in good yields (Scheme 3).

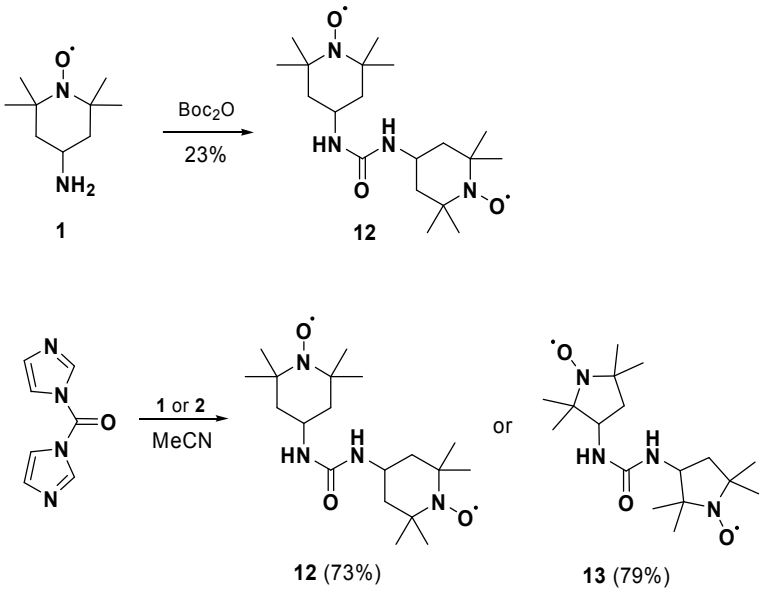

Scheme 3. Optimised synthesis of dinitroxides **12** and **13**.

Having prepared the desired amidic mono-/biradicals **4–13**, we investigated their spectroscopic (EPR) and electrochemical (CV) properties. In addition, we have screened all compounds *in vitro* for their potentially useful antimicrobial activities. We have also performed single-crystal X-ray analyses of mono-/dinitroxides **4**, **5**, **8**, **10**, **11** and elucidated their solid state structures.

Cyclic voltammetry. The redox potentials of the mono-/biradicals **4**–**13** were determined by cyclic voltammetry (CV) in phosphate buffer solution (PBS, pH 7.0), using a paraffine impregnated graphite electrode (PIGE).[5] In general, nitroxides are readily electrochemically oxidised to the corresponding *N*-oxoammonium cations.[22] Cyclic voltammograms of **4**–**13** (Figure S1 in Supporting Information) reveal that all of the studied compounds undergo an one-electron transfer process with half-wave potentials ($E_{1/2}$) in the range of 582–669 mV *vs*. Ag/AgCl electrode (Table 1).

Table 1. Experimental redox potentials and current responses of nitroxide/*N*-oxoammonium cation redox couples.

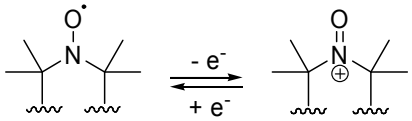

Nitroxide	E_{pa} (mV)[a]	E_{pc} (mV)[b]	$E_{1/2}$ (mV)[c]	ΔE (mV)[d]	I_{pa}/I_{pc}[e]
1[23-26]	652	582	617	69	1.0
AA-TEMPO[24,27]	620	550	585	70	1.0
2[28]	684	556	620	128	1.1
3[5]	574	466	520	108	1.2
4	638	538	588	100	1.9
5	680	526	603	154	1.3
6	695	515	605	180	2.1
7	650	538	594	112	1.5
8	668	538	603	130	1.5
9	692	584	638	108	1.6
10	685	545	615	140	1.5
11	731	607	669	124	2.0
12	633	531	582	102	2.0
13	628	554	591	75	1.9

[a] E_{pa} = anodic peak potential. [b] E_{pc} = cathodic peak potential. [c] $E_{1/2} = (E_{pa} + E_{pc})/2$. [d] $\Delta E = E_{pa} - E_{pc}$. [e] I_{pa} = anodic peak current, I_{pc} = cathodic peak current.

Interestingly, while majority of prepared monoradicals (**5**, **7**–**9**) showed a (quasi)reversible redox properties (**4** and **6** being exceptions) as reflected by approximately equal anodic and cathodic peak currents values (I_{pa}/I_{pc} ~ 1.3–1.6, Table 1), all biradicals (**11**–**13**) except one (**10**) exhibited current intensities sufficiently far from equal (I_{pa}/I_{pc} ~ 1.9–2.0, Table 1), and thus, indicating a significant loss of the kinetic reversibility.[29] However, the cyclic voltammograms of mononitroxides **4**–**9** and dinitroxides **10**–**13** are analogous throughout the series (Figure S1 in Supporting Information), thus demonstrating that electrochemical oxidation of biradicals **10**–**13** likely involves simultaneous one-electron transfer to both radical centers rather than a stepwise process. Moreover, CV results again confirmed a recently postulated[9d] and experimentally observed[5] trend that the presence of electron-withdrawing substituents tends to increase the oxidation potential of a nitroxide in comparison to electron-donating groups (*cf*.: **1** *vs*. **8**, **2** *vs*. **9**, **10** *vs.* **11**, Table 1). In addition, we have observed an exceptionally high values of anodic, cathodic and half-wave potentials for biradical **11** (E_{pa} = 731, E_{pc} = 607, $E_{1/2}$ = 669 mV). However, this particular dinitroxide also features not only a large separation of its redox potentials (ΔE = 124 mV) in comparison to the theoretical Nernstian value (59 mV), but also a non-equal ratio of anodic and cathodic peak currents (I_{pa}/I_{pc} = 2).

EPR spectroscopy. EPR spectra of mononitroxides **4**–**9** measured in dichloromethane (DCM) at 295 K under argon are characteristic of typical three-line signals reflecting the interaction of the unpaired electron with ^{14}N nucleus (A_N) with poorly resolved hyperfine structure caused by ^{1}H or ^{13}C nuclei (A_X). The experimental EPR spectra along with their simulations

are depicted in Figure S2 (see Supporting Information). The spin Hamiltonian parameters elucidated from the simulation of the experimental EPR spectra are summarised in Table 2.

Table 2. Hyperfine coupling constants (mT, accuracy ± 0.001) and *g*-values (accuracy ± 0.0001) elucidated from the simulation of the experimental EPR spectra of monoradicals **4**–**9** measured in DCM at 295 K under Ar.

Nitroxide	A_N (mT)	A_X (mT)	*g*-value
4	1.581	–	2.0061
5	1.583	0.047 (6H), 0.037 (6H) 0.016 (2H), 0.004 (2H)	2.0061
6	1.581	0.043 (6H), 0.040 (6H) 0.017 (2H), 0.011 (2H)	2.0061
7	1.581	0.042 (6H), 0.040 (6H) 0.017 (2H), 0.010 (2H)	2.0061
8	1.573	0.045 (6H), 0.038 (6H) 0.016 (2H), 0.005 (2H)	2.0061
9	1.444	0.892 (4^{13}C), 0.500 (4^{13}C)	2.0058

In contrast to mononitroxides **4**–**9**, the EPR spectra of dinitroxides **10**–**13** obtained in DCM under argon at 295 K revealed different splitting patterns (Figures 3 and 4), thus reflecting the variations in their structures. The spin Hamiltonian for a nitroxide biradical can be constructed with the terms representing the electron Zeeman interactions with external magnetic field, the hyperfine interactions of each electron with the nuclear spins, and the exchange coupling of the two electron spins (Equation 1):[30a]

$$H = g^{(1)}\beta_e B S_z^{(1)} + g^{(2)}\beta_e B S_z^{(2)} + A^{(1)} I_z^{(1)} S_z^{(1)} + A^{(2)} I_z^{(2)} S_z^{(2)} + J S_z^{(1)} S_z^{(2)} \quad (1)$$

where $g^{(1)}\beta_e B S_z^{(1)} + g^{(2)}\beta_e B S_z^{(2)}$ is the Zeeman coupling between the unpaired electrons spin and the magnetic field *B;* $A^{(1)} I_z^{(1)} S_z^{(1)} + A^{(2)} I_z^{(2)} S_z^{(2)}$ is the hyperfine interaction of the electron

spins with magnetically active nuclei, one ^{14}N nucleus characterized with hyperfine coupling constant $A_N^{(1)}$ or $A_N^{(2)}$ is considering in the vicinity of one unpaired electron for dinitroxide; and the last component $JS_z^{(1)}S_z^{(2)}$ represents the exchange coupling between two electron spins, where *J* is the exchange coupling constant.[30b]

For the dinitroxides possessing two symmetric nitroxide moieties in the isotropic solutions the *g*-values in the spin Hamiltonian may be identical ($g^{(1)} = g^{(2)}$), along with the same values of nitrogen hyperfine coupling constants ($A_N^{(1)} = A_N^{(2)}$). However, the specific interactions of NO$^{\bullet}$ group with solvent molecules may caused small asymmetry ($g^{(1)} \neq g^{(2)}$ and $A_N^{(1)} \neq A_N^{(2)}$) also for symmetric dinitroxide molecules.[5,30]

In general, the EPR spectra of nitroxide biradicals are substantially influenced by the value of exchange coupling constant.[30] Two limiting situations may be considered here: $J = 0$ where each nitroxide moiety separately contributes to the EPR signal giving three-line spectrum (intensity ratio 1:1:1), and $J >> A_N$ representing the interacting electrons with five-line EPR spectrum (intensity ratio 1:2:3:2:1). However, if $J \sim A_N$ the EPR spectra of dinitroxides are complex as shown in Figure 3 for dinitroxide **12**.

The data elucidated from the simulation of the experimental EPR spectra of dinitroxides **10**–**13** measured in DCM under argon at 295 K are summarised in Table 3.

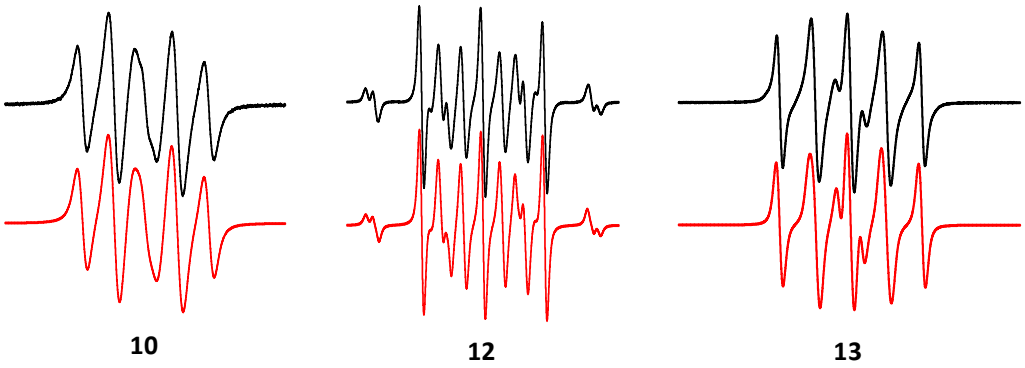

Figure 3. Experimental (–) and simulated (–) X-band EPR spectra of dinitroxides **10**, **12** and **13** obtained at 295 K in DCM. Magnetic field sweep 7 mT; dinitroxide concentration 0.1 mM.

Table 3. Hyperfine coupling constants (mT, accuracy ± 0.001), exchange coupling constant (MHz, accuracy ± 10%) and *g*-values (accuracy ± 0.0001) elucidated from the simulation of the experimental EPR spectra of biradicals **10–13** measured in DCM at 295 K under argon, along with the averaged *g*-values (g_{av}).

Nitroxide	A_N (mT)	*J* (MHz)[b]	*g*-value	g_{av}
10	1.521, 1.642	~360	2.0064, 2.0067	2.0066
11	1.639, 1.539[a]	~410	2.0064, 2.0065	2.0065
	1.486[a]	0	2.0063	2.0063
11[c]	1.552, 1.530[a]	~240	2.0067, 2.0065	2.0066
	1.443[a]	0	2.0064	2.0064
11[d]	1.582, 1.590[a]	~350	2.0065, 2.0062	2.0064
	1.506[a]	0	2.0062	2.0062
12	1.586, 1.585	~50	2.0068, 2.0061	2.0065
13	1.370, 1.549	~430	2.0060, 2.0063	2.0062

[a] Superposition of the signals of interacting and non-interacting biradicals of amide **11**.
[b] 1 mT = 28.0 MHz (*g* = 2).
[c] Measured in *n*-heptane at 295 K.
[d] Measured in dimethylsulfoxide at 373 K.

Thus, the five-line EPR spectrum of biradical **10** corresponds well to the value $J/A_N > 10$ (Figure 3, Table 3); the asymmetry found for A_N couplings is most probably caused by the interaction of nitroxide moieties with polar solvent molecules (DCM); an associated phenomenon was generally observed earlier by others[30] and confirmed recently by our DFT and/or MP2 calculations.[5] On the other hand, in order to fit with the experiment, the simulated EPR spectrum of **11** (Figure 4) was constructed as a superposition of two different signals corresponding to an interacting and non-interacting radicals[31] within the molecule of respective dinitroxide. In order to obtain more information about the potential influence of the conformational dynamics of dinitroxide **11** in solutions, we measured its EPR spectra at 295 K in non-polar *n*-heptane, as well as in more viscous and polar dimethylsulfoxide within the temperature range of 298 K–373 K (Figure 4). The EPR spectrum of **11** measured in *n*-heptane is compatible with the spectrum measured in DCM under identical experimental conditions, and thus, representing the superposition of two individual signals. Due to the reduced solvent polarity, the nitrogen hyperfine couplings in *n*-heptane are lower, and the differences between individual $A_N^{(i)}$ and $g^{(i)}$ are not noticeable (Table 3). Three-line signal of the non-interacting component (J=0) dominates the EPR spectrum of **11** measured at room temperature in viscous DMSO, while the conformers ratio comparable with the one observed in DCM or *n*-heptane was obtained only at 373 K in DMSO (Figure S3 in Supporting Information). Interestingly, the original conformers ratio of 1:1 found in the freshly prepared DCM solution of **11** was changed to ratio of 1:3 in the DCM solution stored for one month at +4 °C (Figure S4 in Supporting Information).

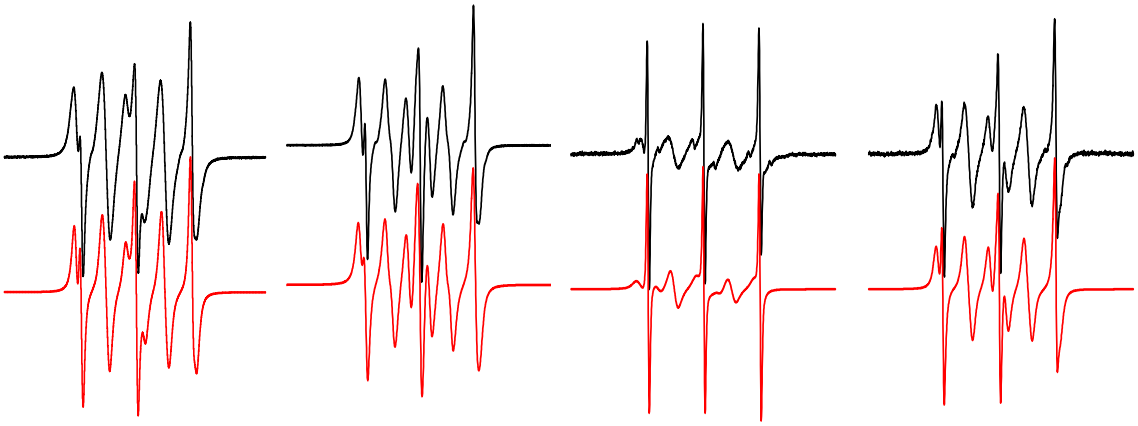

(a) (b) (c) (d)

Figure 4. Experimental (**–**) and simulated (**–**) X-band EPR spectra of dinitroxide **11** (magnetic field sweep 7 mT; dinitroxide concentration 0.1 mM) obtained under Ar at 295 K in: (a) DCM at 295 K, (b) *n*-heptane at 295 K, (c) DMSO at 295 K, and (d) DMSO at 373 K.

Moreover, the influence of 6- *vs.* 5-membered ring on EPR spectra of biradicals **12** and **13** was analysed. While *N*,*N*'-*bis*-TEMPO urea **12** is characterised by limited exchange coupling between two nitroxide moieties (J/A_N ~ 1), and thus, shows a rather complex[32] EPR spectrum (Figure 3), the five-line EPR spectrum of *N*,*N*'-*bis*-PROXYL urea **13** was successfully simulated with J/A_N > 10 (Table 3). Here, the diminished exchange coupling obtained for biradical **12** probably reflects the increased distance[33] between its two nitroxide groups in comparison to biradical **13**.

X-ray diffraction studies. In order to get a detailed insight into the molecular and bulk structures of the studied mono-/biradicals in the solid phase, the X-ray analyses of single crystals of mononitroxides **4**, **5**, and **8** as well as dinitroxides **10** and **11** were performed (the crystallographic data are summarised in Table S1 in Supporting Information). The ORTEP

drawings of elucidated crystal structures are depicted in Figures 5–9. As expected, the piperidine rings in all of these compounds exhibit a chair conformation. Moreover, all nitroxides are stabilised by networks of intra-/intermolecular hydrogen bonds and/or weak interactions in their crystal packings (Figures S5–S14 in Supporting Information). The selected parameters of hydrogen bonds and interactions are summarised in Table S2 (see Supporting Information). In all studied cases, the nitroxyl N–O$^{\bullet}$ bond lengths follow a standard interatomic distance (~ 1.28 Å, Table 4) observed for similar TEMPO derivatives.[5] While the amidic C=O bond lengths in nitroxides **4**, **8**, **10** and **11** fall into the range of 1.20–1.25 Å usually observed for carbonylamino groups,[34] an analogous interatomic distance in carbamate **5** (1.191(3) Å) is expectedly shorter (Table 4). Accordingly, the C–N bond distances of carbonylamino groups in all studied nitroxides are in the standard range of 1.32–1.38 Å usually observed[34] for carboxamides (Table 4).

Table 4. Comparison of bond lengths obtained from X-ray analyses.

Nitroxide	N–O$^{\bullet}$ (Å)	C=O (Å)	C–N (Å)
4	1.283(2)	1.220(2)	1.318(2)
5	1.285(2)	1.191(3)	1.327(3)
8	1.288(3)	1.203(4)	1.324(4)
10	1.282(2)	1.222(2)	1.360(2)
11[a]	1.282(2)	1.218(3)	1.342(3)

[a)] The crystal of dinitroxide **11** included ethanol and water as solvent molecules (**11·0.5EtOH·0.5H_2O**).

Due to the significant rotational flexibility of the *tert*-butyl group in amide **4** (Figure 5) the X-ray analysis furnished an ORTEP with disordered parts (Figure S5 in Supporting Information). From the bulk point of view, single molecules of mononitroxide **4** are interconnected *via*

hydrogen bonds between carboxamide group into the supramolecular *C*(4) chains[35] with H···O distance of 2.120 Å (Figure S6 in Supporting Information).

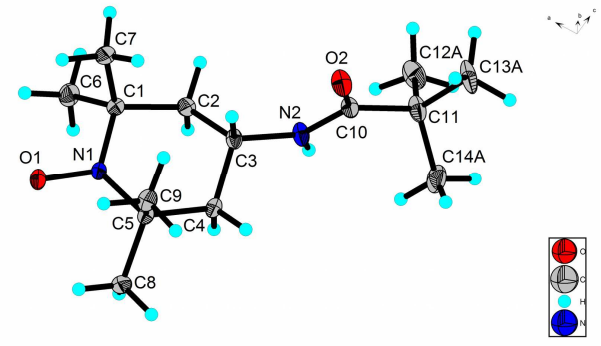

Figure 5. ORTEP drawing of mononitroxide **4**.

The symmetrical molecule of mononitroxide **5** (Figure 6) lies in mirror spaces and two halves of the molecule occupy independent parts of the cell. The bulk structure of **5** is stabilised by both intermolecular NH···O hydrogen bond between the nitroxyl and carbamate moieties (2.055 Å), and three types of H···H intermolecular contacts (H2B and H4B, H8B and H5A, H5B and H9A) with interatomic distances in the range of 2.474–2.870Å (Figure S7 in Supporting Information).

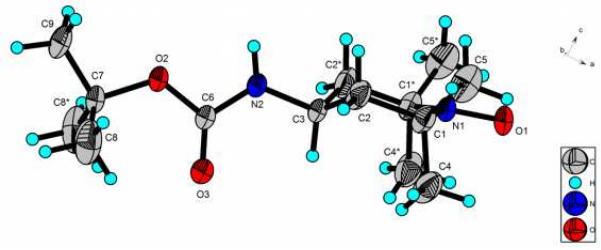

Figure 6. ORTEP drawing of mononitroxide **5**.

Analogously to **5**, the symmetrical molecule of mononitroxide **8** (Figure 7) also lies in mirror spaces and two halves of the molecule occupy independent parts of the cell. Moreover, due to the rotational flexibility of the CF_3-group, the X-ray analysis of trifluoroacetamide **8**

furnished an ORTEP with disordered parts (Figure S8 in Supporting Information). The bulk structure of **8** consists of *zig-zag* 1-D supramolecular *C*(7) chains[35] formed by intermolecular NH···O hydrogen bonds between the nitroxyl and amide moieties with a distance of 2.000 Å (Figure S9 in Supporting Information). The molecular network of **8** also features a weak C–H···O hydrogen bonds with interatomic distances of 2.636 and 2.717 Å, respectively.

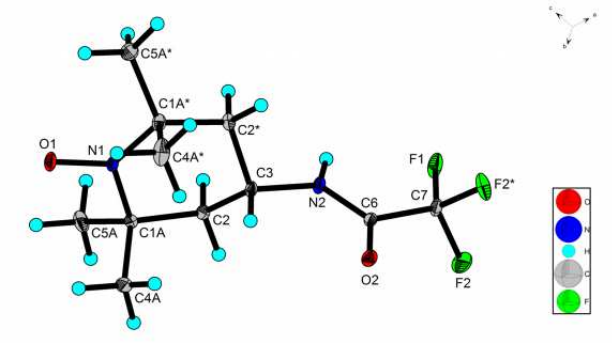

Figure 7. ORTEP drawing of mononitroxide **8**.

The bulk structure of dinitroxide **10** (Figure 8) is stabilised by intramolecular H···H interaction with very short interatomic distance of 1.978 Å (between H12A and H2B) and seven intermolecular interactions: between the nitroxyl's oxygen and hydrogen atoms H6B, H20B, H16B, H17A (2.469–2.822 Å), between amidic oxygen O3 and H4A (2.672 Å), H15A and H18B, H13B with interatomic distances of 2.420 and 2.325 Å (Figures S10–S12 in Supporting Information).

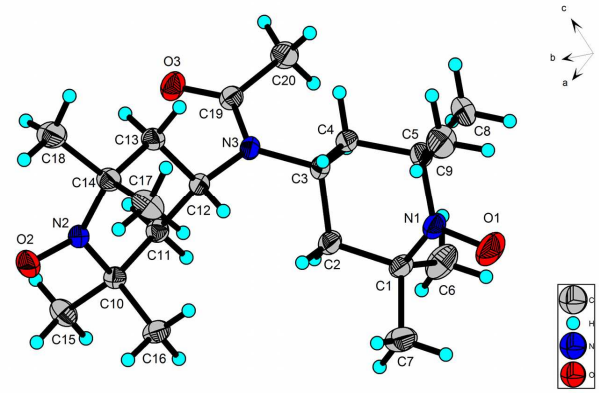

Figure 8. ORTEP drawing of dinitroxide **10**.

The X-ray analysis of a crystal obtained by slow evaporation of wet ethanolic solution of dinitroxide **11** (Figure 9) revealed that both EtOH and H_2O were incorporated into the solid during its formation to yield **11·0.5EtOH·0.5H$_2$O**. Due to the rotational flexibility of the CF_3-group, the X-ray analysis of trifluoroacetamide **11** furnished an ORTEP with disordered parts (Figure S13 in Supporting Information). On the other hand, the disordered solvent molecules around special position are connected to the dinitroxide **11** through O1W–H1WA···O1S, O1W–H1WB···O2 and O1S–H1S···O1W hydrogen bonds with H···O distances in the range of 2.190–2.390 Å. The O–H···O network is completed by weak C7–H7A···O1S hydrogen bond with H7A···O1S distance of 2.571 Å (Figure S14 in Supporting Information). Regarding the bulk structure, the molecules of **11** are linked through weak C2–H2B···O3 and C11–H11B···F2A interactions the into supramolecular *zig-zag* chains with H···O/F distances of 2.564 and 2.615 Å, respectively.

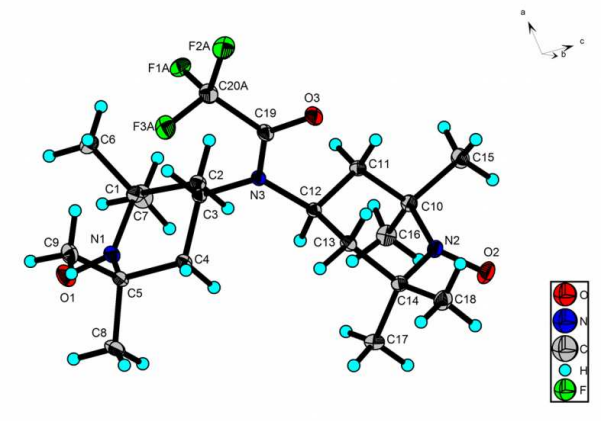

Figure 9. ORTEP drawing of dinitroxide **11·0.5EtOH·0.5H_2O**. The solvent molecules (EtOH and H_2O) were omitted for clarity.

Antimicrobial assays *in vitro*. The prepared mononitroxides **4–9** and dinitroxides **10–13** were also tested for their *in vitro* antimicrobial activity (Table 5) using bacteria (*Staphylococcus aureus, Staphylococcus epidermidis, Proteus* sp.), yeast (*Candida albicans, Candida parapsilosis*) and filamentous fungi (*Fusarium culmorum, Botrytis cinerea, Aspergillus fumigatus*). Considering the antibacterial properties, while all the nitroxide radicals displayed a growth inhibition of prokaryotic Gram-positive *S. epidermidis* (58–88%) and/or *S. aureus* (10–79%), the gama-proteobacteria *Proteus* sp. was fully resistant to all but one tested compound (22% growth inhibition with dinitroxide **10**) even at 1 mM concentration. Interestingly, the mononitroxide **8** was highly selective against *S. epidermidis* (IC_{50} 0.5 mmol/L). In general, this bacterial strain was sensitive towards all piperidinyl nitroxides with the highest antimicrobial effect observed for **5**, **6**, **10**, and **11**. In contrast, neither of the two pyrrolidinyl derivatives **9** and/or **13** were capable to inhibit the growth of *S. epidermidis*. This observation clearly points to the importance of TEMPO over PROXYL skeleton in order to suppress this particular bacterial strain. In addition, piperidinyl dinitroxides **10** and **11** were also active against *S. aureus* (Table 5).

Table 5. The inhibitory effect of mono-/dinitroxides **4**–**13** on the growth of *Staphylococcus* sp.

Nitroxide	*S. aureus*		*S. epidermidis*	
	Inhibition[a] (%)	IC_{50}[b] (mmol/L)	Inhibition[a] (%)	IC_{50}[b] (mmol/L)
4	10	> 1	69	0.4
5	31	> 1	88	< 0.05
6	24	> 1	75	0.09
7	13	> 1	58	0.6
8	0	> 1	66	0.5
9	12	> 1	0	> 1
10	74	0.3	75	0.07
11	79	0.05	84	< 0.05
12	19	> 1	65	0.6
13	21	> 1	0	> 1

[a)] Growth inhibition determined at 1 mmol/L concentration of the tested compound.

[b)] In all cases, the corresponding MIC values were higher than 1 mmol/L.

Moreover, we have found an interesting correlation[36] between the electronic characteristics of substituents at position C-4 of the piperidine ring (reflected by redox potentials) of TEMPO derivatives **6**–**8**, **10**–**12** and their *in vitro* inhibition activity against *S. epidermidis* (Figure 10). It is clear that the more electron-withdrawing substituents (*cf.* **7** *vs.* **8**, **10** *vs.* **11**) and/or more TEMPO units (*cf*. **8** *vs.* **11**) are present in the respective nitroxide the stronger is the bacterial growth inhibition. As the anodic potential reflects the ability of a nitroxide to transfer its unpaired electron(s), it appears that stronger is the reductant (higher E_{pa}) the better is the growth inhibition (higher PGI). We speculate that such a relationship might suggest a mechanism of antibacterial action *via* an induction/promotion of complex oxidative burst involving highly reactive ROS species.[37]

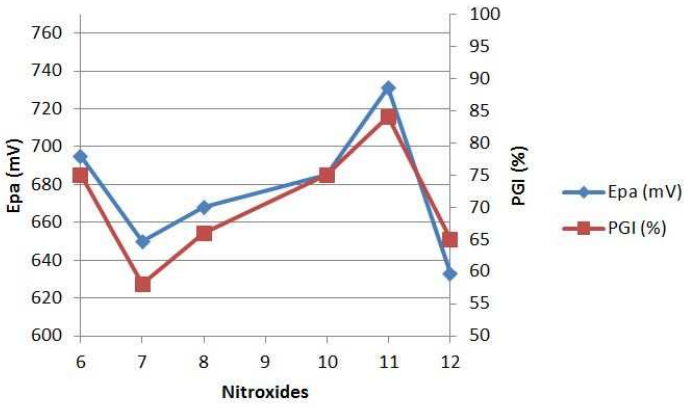

Figure 10. Correlation of the anodic potential (E_{pa}) of piperidine nitroxides **6**–**8**, **10**–**12** with their growth inhibition (PGI) of *S. epidermidis*.

Regarding the antifungal properties,[38] mono/dinitroxides **4**–**13** showed only weak to moderate activity. Even though complete growth inhibition was not observed in the range of tested concentrations, however, derivates **7** and **11** have partially suppressed the growth of *F. culmorum* (~ 50% inhibition), analogously to the compound **6** that was moderately active against *B. cinerea*. On the other hand, however, all tested compounds generally showed only (very) weak inhibition activity towards *A. fumigatus* (Table 6). Finally, model yeasts were primarily resistant to any of the tested mono/dinitroxides (0–17% inhibition at 1 mmol/L) except biradical **13** that was able to partially suppress the growth of *C. parapsilosis* (27% inhibition).

Table 6. The inhibitory effect of mono-/dinitroxides **4**–**13** on the growth of filamentous fungi.

Nitroxide	Inhibition[a,b] (%)		
	F. culmorum	*B. cinerea*	*A. fumigatus*
4	11	13	7
5	27	17	11
6	21	50	15
7	51	8	7
8	16	4	9
9	22	15	7
10	17	8	9
11	52	27	26
12	7	39	9
13	19	39	9

[a)] Growth inhibition determined at 1 mmol/L concentration of the tested compound.

[b)] In all cases, the corresponding MIC values were higher than 1 mmol/L.

CONCLUSIONS

In conclusion, two comparative sets of mononitroxyl amides/carbamate **4**–**9** and dinitroxyl amides/ureas **10**–**13** were designed and prepared. These novel TEMPO and/or PROXYL derivatives were fully characterised and some of their solid structures were determined by single crystal X-ray analyses. The spin and redox properties of all compounds were studied by means of EPR spectroscopy and cyclic voltammetry. In addition, their antimicrobial properties were also investigated. Regarding CV, all studied radicals undergo one-electron transfer process with half-wave potentials in the range of 582–669 mV. The results confirmed an emerging trend that the presence of electron-withdrawing substituents on the saturated *N*-heterocyclic skeleton tends to increase the oxidation potential of a nitroxide in comparison to electron-donating groups. While EPR spectra of monoradicals **4**–**9** in DCM feature the typical three-line signal, spectra of biradicals **10**–**13** revealed more complex splitting patterns. These are most probably caused by the intermolecular interactions of

nitroxide moieties with polar solvent molecules and/or conformational flexibility of two radical centres within respective molecules. Moreover, the increased distance between two radical sites in *bis*-TEMPO *vs. bis*-PROXYL derivatives also influences the complexity of EPR spectra of the former ones. Finally, we have determined the *in vitro* antimicrobial activity of prepared nitroxides. Unlike pyrrolidinyl derivatives, all piperidinyl radicals significantly inhibit the growth of *Staphylococcus* sp. Interestingly, the more electron-withdrawing substituent is present on the piperidine ring, the stronger is the antibacterial effect of the respective nitroxide against *S. epidermidis*. On the other hand, all tested radicals displayed only weak growth inhibition of yeast and/or filamentous fungi.

EXPERIMENTAL SECTION

General: *Synthesis:* All solvents of *p.a.* purity were dried over 4Å molecular sieves. All other reagents were purchased and used without further purification. Thin layer chromatography (TLC) was performed on aluminium plates pre-coated with 0.2 mm silica gel 60 F254. Flash column liquid chromatography (FLC) was performed on Kieselgel 60 (40-63 μm). Infrared (IR) spectra were recorded on a FTIR spectrometer as films on a diamond sampler (ATR). Melting points were determined on capillary apparatus and are uncorrected. Liquid chromatography mass spectrometry (LC-MS) analyses were performed on an instrument quipped with a multimode MS detector using the MM ESI/APCI ionisation method (column: Zorbax SB C-8 12.5 _ 2.1 mm, particle size 5 μm, eluent: water / MeOH with 0.1% HCO_2H, gradient 0–100% of MeOH for 2.5 min, flow 1.5 mL/min). HRMS spectra were recorded on TOF-Q instrument and evaluated using Compass DataAnalysis 4.0 software. Elemental analysis was carried out

at the Department of Inorganic Chemistry, Slovak University of Technology in Bratislava, Slovakia.

***N*-(1-Oxo-2,2,6,6-tetramethylpiperidin-4-yl)-pivalamide (4):** Prepared accordingly to the described procedure.[17] Product was isolated as pale orange solid (714 mg, 87 %). Crystallisation of small amount of **4** from chloroform/hexanes gave orange crystals suitable for X-ray analysis (Figure 5).

For **4**: R_F = 0.64 (EtOAc), mp 179-180 °C [Ref.[17] 179 °C]; ESI-MS (*m/z)* = 256.20 $[M+1]^+$; IR (ATR): ν_{max} 3332, 2972, 2939, 2868, 1631, 1538, 1477, 1464, 1362, 1322, 1213, 1088, 887, 670, 582 cm^{-1}; Anal. Calcd. for $C_{14}H_{27}N_2O_2^{\bullet}$ (255.21): C 65.84, H 10.66, N 10.97. Found C 65.89, H 10.65, N 10.93.

4-*tert*-Butoxycarbonylamino-2,2,6,6-tetramethylpiperidin-1-oxid (5): Prepared accordingly to the described procedure.[18] Product was isolated as pale orange solid (317 mg, 91 %). Crystallisation of small amount of **5** from a ^{i}octane/chloroform solution (1:1) gave orange crystals suitable for X-ray analysis (Figure 6).

For **5**: R_F = 0.85 (EtOAc), m.p. 197-200 °C [Ref.[18] 199 °C]; ESI-MS (*m/z)* = 272.3 $[M+1]^+$; IR (ATR) ν_{max} 3300, 2970, 2942, 1701, 1531, 1459, 1363, 1309, 1240, 1167, 1133, 1014, 900, 869, 638, 569 cm^{-1}; Anal. Calcd. for $C_{14}H_{27}N_2O_3^{\bullet}$ (271.20): C 61.96, H 10.03, N 10.32. Found C 61.91, H 9.80, N 10.03.

***N*-(1-Oxo-2,2,6,6-tetramethylpiperidin-4-yl)-benzoylamide (6):** 4-amino-TEMPO **1** (171 mg, 1 mmol) was dissolved in toluene (10 mL) and Et_3N (202 mg, 278 μL, 2 mmol) was added.

Reaction mixture was cooled in water bath (15 °C) and a solution of benzoyl chloride (prepared from benzoic acid (122 mg, 1 mmol) and oxalyl chloride (140 mg, 99 μL, 1.1 mmol) in toluene (10 mL)) was added dropwise. After 2 hrs, DCM (15 mL) and 1 N aq. HCl (10 mL) were added and the mixture was left to stir for 5 min. The organic phase was separated, dried over anhydrous Na_2SO_4, filtered and evaporated *in vacuo*. Purification by FLC furnished **6** (235 mg, 85 %) as orange solid.

For **6**: R_F = 0.46 (EtOAc/Hexanes 1/2), mp 130-132 °C; ESI-MS (*m/z)* = 276.2 $[M+1]^+$; IR (ATR) ν_{max} 3415, 3352, 3269, 2976, 2933, 1629, 1545, 1491, 1460, 1331, 1242, 1178, 1076, 702, 560 cm^{-1}; Anal. Calcd. for $C_{16}H_{23}N_2O_2^{\bullet}$ (275.37): C 69.79, H 8.42, N 10.17. Found C 69.43, H 8.26, N 9.95.

4-Formamido-2,2,6,6-tetramethylpiperidin-1-oxid (7): Prepared accordingly to the described procedure.[19] Product was isolated as pale orange solid (380 mg, 93 %).

For **7**: R_F = 0.17 ($CHCl_3$/EtOAc 1/1), mp 105-107 °C; ESI-MS (*m/z)* = 200.15 $[M+1]^+$; IR (ATR) ν_{max} 3359, 2979, 2935, 2870, 1669, 1508, 1380, 1244, 1209, 1179, 1093, 647, 441 cm^{-1}; Anal. Calcd. for $C_{10}H_{19}N_2O_2^{\bullet}$ (199.15): C 60.27, H 9.61, N 14.06. Found C 60.41, H 9.47, N 14.01.

4-(2,2,2-Trifluoracetylamino)-2,2,6,6-tetramethylpiperidin-1-oxid (8): Modifying the described procedure,[20] nitroxide **8** was prepared by reaction of 4-amino-TEMPO **1** (171 mg, 1 mmol) and Et_3N (203 mg, 280 μL, 2 mmol) with $(CF_3CO)_2O$ (420 mg, 282 μL, 2 mmol) in anhydrous DCM (4 mL). After the reaction was complete (6 hrs, TLC control), the mixture was diluted with DCM (15 mL), washed with 1 N HCl (15 mL), saturated aq. $NaHCO_3$ soln. (15

mL) and dried over anhydrous Na_2SO_4. After filtration, the evaporation of volatiles *in vacuo* and FLC purification afforded an orange solid (178 mg, 84 %). Crystallisation of small amount of **8** from ethanolic solution gave orange crystals suitable for X-ray analysis (Figure 7).

For **8**: R_F = 0.79 (EtOAc/Hexanes 1/1), mp 154-156 °C [Ref.[20] 149-151 °C]; ESI-MS (*m/z)* = 269.14 $[M+2]^+$; IR (ATR) ν_{max} 3282, 3093, 2979, 1724, 1556, 1466, 1365, 1176, 1155, 864, 727, 677, 519 cm^{-1}; HRMS Calcd. for $C_{11}H_{18}F_3N_2O_2^{\bullet}$ 267.1320, Found 267.13183.

3-(2,2,2-Trifluoroacetylamino)-2,2,5,5-tetramethylpyrrolidin-1-oxid (9): 3-amino-PROXYL **2** (400 mg, 1 mmol) and Et_3N (644 mg, 894 μL mmol, 2.5 mmol) were dissolved in anhydrous DCM (20 mL) and $(CF_3CO)_2O$ (1069 mg, 708 μL, 2 mmol) was added dropwise. After the reaction was complete (16 hrs, TLC control), the mixture was washed with 1 N HCl (15 mL), saturated aq. $NaHCO_3$ soln. (15 mL) and dried over anhydrous Na_2SO_4. After filtration, the evaporation of volatiles *in vacuo* and FLC purification afforded **9** (467 mg, 72 %) as a pale yellow solid.

For **9**: R_F = 0.47 (EtOAc/DCM 1/2), mp 119-121 °C; ESI-MS (*m/z)* = 255.11 $[M+2]^+$; IR (ATR) ν_{max} 3329, 2979, 1723, 1703, 1563, 1468, 1365, 1212, 1180, 1152, 879, 681, 664, 518 cm^{-1}; HRMS Calcd. for $C_{10}H_{16}F_3N_2O_2^{\bullet}$ 253.1164, Found 253.11598.

***N*-Acetyl-*N, N*-bis-(1-oxo-2,2,6,6-tetramethylpiperidin-4-yl)-amine (10):** *Bis*-TEMPO-amine **3** (800 mg, 2.46 mmol) was dissolved in DCM (10 mL) and Et_3N (503 mg, 691 μL, 4.92 mmol) was added. Then, Ac_2O (502 mg, 464 μL, 4.92 mmol) was added dropwise and the reaction mixture was stirred for 16 hrs. The mixture was diluted with DCM (10 mL) and water (2 mL) with 1 N HCl (2 mL) were added. The organic phase was separated, washed with saturated

aq. $NaHCO_3$ soln. (10 mL), dried over anhydrous Na_2SO_4, filtered and evaporated *in vacuo*. Purification with FLC afforded **10** (731 mg, 81 %) as orange solid. Crystallisation of small amount of **10** from ^{i}octane/chloroform (1/1) solution gave red crystals suitable for X-ray analysis (Figure 8).

For **10**: R_F = 0.42 (EtOAc/Hexanes 1/2), mp 192-195 °C; ESI-MS (*m/z)* = 368.30 $[M+1]^+$; IR (ATR) ν_{max} 2994, 2935, 1645, 1638, 1466, 1433, 1377, 1364, 1356, 1289, 1238, 1206, 1180, 906, 633, 561 cm^{-1}; Anal. Calcd. for $C_{20}H_{37}N_3O_3^{\bullet\bullet}$ (367.28) C 65.36, H 10.15, N 11.43. Found C 65.22, H 10.23, N 11.38.

***N*-(2,2,2-Trifluoroacetyl)-*N*,*N*-bis-(1-oxo-2,2,6,6-tetramethylpiperidin-4-yl)-amine (11):** *Bis*-TEMPO-amine **3** (150 mg, 0.46 mmol) was dissolved in anhydrous DCM (2 mL) and Et_3N (117 mg, 160 μL, 1.15 mmol) was added. Trifluoroacetic anhydride (194 mg, 128 μL, 0.92 mmol) was added dropwise and the reaction mixture was stirred for 16 hrs. The mixture was diluted with DCM (10 mL) and water (2 mL) with 1 N HCl (2 mL) were added. The organic phase was separated, washed with saturated aq. $NaHCO_3$ soln. (10 mL), dried over anhydrous Na_2SO_4, filtered and evaporated *in vacuo*. Purification with FLC afforded **11** (134 mg, 69 %) as orange oil that slowly solidified upon standing at r.t. in few days. Crystallisation of small amount of **11** from its wet ethanolic solution gave orange-red crystals of **11·0.5H_2O·0.5EtOH** suitable for X-ray analysis (Figure 9).

For **11**: R_F = 0.74 (EtOAc/$CHCl_3$ 1/1), mp 95-97 °C; ESI-MS (*m/z)* = 422.30 $[M+1]^+$; IR (ATR) ν_{max} 2976, 2941, 1684, 1471, 1454, 1364, 1324, 1216, 1191, 1147, 1045, 760, 735, 654, 459 cm^{-1}; HRMS Calcd. for $C_{20}H_{34}F_3N_3O_3^{\bullet\bullet}$ 421.2552, Found 421.2546.

***N,N*-Bis-(1-oxo-2,2,6,6-tetramethylpiperidin-4-yl)-carbamide (12):** Carbonyldiimidazol (213 mg, 1.31 mmol) was mixed with MeCN (6 mL) and solution of 4-amino-TEMPO **1** (450 mg, 2.63 mmol) in MeCN (4 mL) was added dropwise at r.t. After 24 hrs, DCM (10 mL) and 1 N HCl (10 mL) were added and the mixture was stirred for 5 min. The organic phase was separated and water phase was extracted with DCM (2 x 10 mL). The combined organic extracts were dried over anhydrous Na_2SO_4, filtered and evaporated *in vacuo*. Purification by FLC furnished **12** (354 mg, 73 %) as dark orange solid.

For **12**: R_F = 0.31 (EtOAc), mp 200-202 °C [Ref.[39] 203-204 °C]; ESI-MS (*m/z)* = 369.20 $[M+1]^+$; IR (ATR) ν_{max} 3383, 3307, 3271, 2972, 2934, 1728, 1666, 1622, 1558, 1540, 1315, 1231, 1176, 1072, 636, 562, 432 cm^{-1}; Anal. Calcd. for $C_{19}H_{36}N_4O_3^{\bullet\bullet}$ (368.28) C 61.93, H 9.85, N 15.20. Found C 61.71, H 9.79, N 15.18.

***N,N*-Bis-(1-oxo-2,2,5,5-tetramethylpyrrolidin-3-yl)-carbamide (13):** Carbonyldiimidazol (103 mg, 0.64 mmol) was mixed with MeCN (4 mL) and a solution of 3-amino-PROXYL **2** (200 mg, 1.27 mmol) in MeCN (4 mL) was added dropwise at r.t. After 18 hrs, DCM (10 mL) and 1 N HCl (10 mL) were added and the mixture was stirred for 5 min. The organic phase was separated and water phase was extracted with DCM (2 x 10 mL). The combined organic extracts were dried over anhydrous Na_2SO_4, filtered and evaporated *in vacuo*. Purification by FLC afforded **13** (170 mg, 79 %) as dark orange oil that solidified upon standing at r.t.

For **13**: R_F = 0.26 (EtOAc), mp 223-225 °C; ESI-MS (*m/z)* = 341.26 $[M+1]^+$; IR (ATR) ν_{max} 3377, 3356, 3309, 2972, 2933, 2870, 1685, 1625, 1547, 1460, 1363, 1299, 1228, 1104, 752, 593, 550, 469 cm^{-1}; Anal. Calcd. for $C_{17}H_{32}N_4O_3^{\bullet\bullet}$ (340.25) C 59.97, H 9.47, N 16.46. Found C 59.83, H 9.35, N 16.28.

Cyclic voltammetry. *Chemicals:* The stock solutions of compounds **1–13** ($c = 1\times10^{-3}$ mol·L^{-1}) in H_2O/MeOH (9/1, v/v) were used for the preparation of working solutions ($1\cdot10^{-4}$ mol·L^{-1}) for electrochemical measurements by dilution with aq. phosphate buffer solution (PBS) at pH = 7 as supporting electrolyte. The latter was prepared in a usual way by mixing an appropriate amount of monosodium phosphate monohydrate ($NaH_2PO_4\cdot H_2O$) and disodium phosphate heptahydrate ($Na_2HPO_4\cdot 7H_2O$). All chemicals (analytical-reagent grade) were used without further purification. The aqueous solutions were made with double-distilled deionised water with resistivity above 18 MΩcm.

Electrochemical measurements: The cyclic voltammetry (CV) measurements were performed using an AUTOLAB PGSTAT-302N (Metrohm Autolab B.V., The Netherlands) potentiostat/galvanostat equipped with USB electrochemical interface connected to three-electrode single compartment glass cell and personal computer for data storage and processing. NOVA 1.9 software was employed for elaboration and evaluation of all CV voltammograms. The glass electrochemical cell consisted of Ag/AgCl (3 mol·L^{-1} KCl) and Pt wire as reference and counter electrode, respectively. Paraffine impregnated graphite electrode (PIGE) with diameter of 5 mm was used as working electrode. The PIGE was polished with aluminium oxide (grain size = 0.3 μm) and rinsed with deionised water to obtain the fresh electrode surface before each experiment. The pH value of PBS was monitored with pH meter Model 215 (Denver Instrument, USA) with combined glass electrode, which was regularly calibrated with standard buffer solutions. All the half-wave potentials ($E_{1/2}$) are given against Ag/AgCl (3 mol·L^{-1} KCl) reference electrode at an ambient temperature of 25±1 °C. The 20 mL of the supporting electrolyte containing an appropriate

amount of studied compound was added to the glass electrochemical cell. Before each measurement, ultrapure N_2 (O_2 < 2 ppm) was used to degass the solutions (10 min) and to provide an inert atmosphere inside the electrochemical cell. CV voltammograms were recorded in a potential range from -1 to +1 V with the use of optimised instrumental parameters as follows: scan rate of 0.1 V s^{-1}, step potential of 0.005 V and interval time of 0.05 s. At the beginning, the current response for a blank (PBS at pH = 7 without the presence of any studied nitroxide) was measured to check the electrochemical background of the system. Subsequently, CV voltammograms of each studied species were carried out fivefold (n = 5) and the average scan was considered for the evaluation of $E_{1/2}$ and construction of CV figures.

Electron Paramagnetic Resonance. The stock solutions of all nitroxides were prepared in anhydrous dichloromethane (Merck, SeccoSolv®, max. 0.004% H_2O), dimethylsulfoxide (Merck, SeccoSolv®, max. 0.025% H_2O) and/or *n*-heptane (Merck, Uvasol®). EPR spectra were measured with freshly diluted solutions (*c* 0.1 mM) carefully saturated with argon and immediately transferred to a small quartz flat cell (WG 808-Q, Wilmad-LabGlass, USA) optimised for the TE_{102} cavity (Bruker, Germany). The X-band spectra were recorded using a EPR spectrometer EMX Plus (Bruker, Germany) at 295 K; in DMSO the EPR spectra were measured within the temperature range of 298 K–373 K. The temperature was set using a Bruker temperature control unit ER 4111 VT. The *g*-values were determined using a built-in magnetometer. Typical EPR spectrometer settings were the following: microwave frequency: 9.428 GHz; microwave power: 1.053 mW or 10.53 mW; center field: 335.8 mT; sweep width:

6–10 mT; gain: 5×10^3; modulation amplitude: 0.02 mT; scan: 82 s; time constant: 10.24 ms; number of scans: 5.

The experimental EPR spectra were analysed and simulated using the Bruker software WinEPR and SimFonia, Winsim2002 software.[40] The simulated spectra of dinitroxides were calculated with EasySpin software package[41] using the fitting function pepper suitable for the exchange coupling constant calculation in systems with S > 1/2.

X-ray analyses. Single-crystal X-ray diffraction experiments were made at the 293(1) K temperature on Oxford Gemini R (for **5** and **10**) or Xcalibur S (for **4**, **8**, and **11·0.5EtOH·0.5H_2O**) four circle κ-axis diffractometers equipped with Ruby or Sapphire 2 CCD detectors and graphite monochromated Mo Kα radiation. Crystal data, data collection procedures, structure determination methods and refinement results are summarised in Table S1 (see Supporting Information). CrysAlis program package[42] was used for data reduction. The structures were solved by direct methods using programs Shelxs97[43] and SIR2011,[44] or charge-flipping method using program OLEX2.SOLVE.[45] Refinement was carried out on F^2 and scattering factors were incorporated in ShelxL97, ShelxL2013 or OLEX2.REFINE programs[45,47] were used. All non-hydrogen atoms were refined with anisotropic thermal parameters. All hydrogen atoms were found from the Fourier map and they were refined isotropically. The Diamond program package was used for molecular structure drawing.[46] The *tert*-butyl group in mononitroxide **4** displaying a positional disorder (Figure S3 in Supporting Information) was modelled in three positions using OLEX program package[45] with occupancy factors of 0.62, 0.22 and 0.16.

The trifluoromethyl group in mononitroxide **8** is disordered around special positions of mirror. The discrete positional disorder of *gem*-dimethyl groups of **8** was also observed (Figure S6 in Supporting Information). The trifluoromethyl group of **11·0.5EtOH·0.5H$_2$O** is also disordered in two positions (Figure S11 in Supporting Information) with occupancy factors 0.67 and 0.33. The F and C atoms of disordered groups were modelled using DFIX and SADI restrains. The disordered ethanol in the structure of **11·0.5EtOH·0.5H$_2$O** residing in the special position (PART -1) was calculated using FRAG 17, FEND and AFIX 176 commands and ethanol molecule coordinates from Idealized Molecular Geometry Library.[47]

The atomic displacement parameters of C, O and F atoms were restrained using RIGU[48] and SIMU commands, and for some atoms were also constrained using EADP command.

Crystallographic data for the structural analyses have been deposited with the Cambridge Crystallographic Data Centre CCDC No.: 953446 (for **4**), 953447 (for **5**), 953448 (for **8**), 953449 (for **10**), and 953450 (for **11·0.5EtOH·0.5H$_2$O**). Further details of the crystal structures investigations are available free of charge via www.ccdc.cam.ac.uk/conts/retrieving.html (or from the CCDC, 12 Union Road, Cambridge CB2 1EZ, UK; +44 1223 336033; e-mail: deposit@ccdc.cam.ac.uk)

Biological assays. The antibacterial activity of newly synthetised TEMPO radicals was evaluated by a broth micro-dilution method adapted from previous studies and in accordance to the NCCLS guidelines[49] on G$^+$ bacteria *Staphylococcus epidermidis* (Collection of Microorganisms at the Department of Biochemistry and Microbiology STU in Bratislava, Slovakia), *Staphylococcus aureus* CCM 3953 and G$^-$ bacteria *Proteus* sp. CCM 1977 (Czech Collection of Microorganisms, Masaryk University, Brno, Czech Republic).

Bacteria were grown in Mueller Hinton broth at 37 °C until an optical density (OD) of 0.8 at a wavelength of 630 nm. The bacterial cultures were adjusted to equal the McFarland No. 0.5 turbidity standard. Final inoculum was prepared by diluting the adjusted bacterial suspension at 1:100 with Mueller Hinton broth, 198 μL of inoculated broth was transferred to each well of the 96-well plate that contained 2 μL of nitroxide radicals dissolved in DMSO (final concentrations 1 – 0.05 $mmol \cdot L^{-1}$). The inoculated micro-plates were incubated at 37 °C until the growth reached the stationary phase. The antimicrobial activity was characterised by IC_{50} and MIC values that were read from toxicity curves. The MIC was defined as the lowest concentration of the compound that inhibited the growth.

The antifungal assay was done on yeasts and filamentous fungi. Yeasts *Candina albicans* SC 5314 and *Candida parapsilosis* ATCC 22019 (American Type Culture Collection) were tested analogously as the antibacterial activity, however, the yeasts were grown in Sabouraodo broth. The antifungal activity was evaluated based on IC_{50} and MIC_{80} values.[50]

Model filamentous fungi *Aspergillus fumigatus* CCM F-373, *Botrytis cinerea* CCM F-16 and *Fusarium culmorum* CCM F-21 were obtained from Czech Collection of Microorganisms, Masaryk University, Brno, Czech Republic. These were tested by macro-dilution technique on solidified growth medium potato-dextrose agar during static cultivation. Potato-dextrose growth media containing appropriate concentration (1 – 0.1 $mmol \cdot L^{-1}$) of tested nitroxide radicals were inoculated by fungal conidial suspension of tested fungi ($1 \cdot 10^6$ conidia/mL) in the centre of growth media in Petri dishes. Fungi were cultivated[51] at 25 °C for 96 hours. The radial growth was measured in millimeters. All experiments were done in three parallels of two independent experiments.

ACKNOWLEDGMENT

This work was supported by the Science and Technology Assistance Agency under contracts No. APVV-0014-11, APVV-0797-11, APVV-0282-10 and the Grant Agency of the Slovak Republic (VEGA 1/0051/13 and VEGA 1/0289/12).

SUPPORTING INFORMATION

Copies of CV spectra of all nitroxides **4–13**; copies of EPR spectra of mononitroxides **4–9**; EPR spectra of dinitroxide **11** in DCM fresh solution and after 1-month storage at +4 °C, EPR spectra of dinitroxide **11** in DMSO in the temperature range of 298 K–373 K, copies of HRMS spectra of nitroxides **8**, **9** and **11**; ORTEP drawings and/or packing diagrams of nitroxides **4**, **5**, **8**, **10**, **11** and their selected crystallographic data.

REFERENCES

(1) (a) Arends, I. W. C. E.; Yu-Xin, L.; Ausan, R.; Sheldon R. *Tetrahedron* **2006**, *62*, 6659; (b) Yin, W.; Chu, C.; Lu, Q.; Tao, J.; Liang, X.; Liu, R. *Adv. Synth. Catal*. **2010**, *352*, 113.

(2) Montanari, F.; Quici, S.; Henry-Riyad, H.; Tidwell, T. T.; Ed.; 2,2,6,6-Tetramethylpiperidin-1-oxyl. In *Encyclopedia of Reagents for Organic Synthesis*; Wiley-VCH: Weinheim, **2005**.

(3) (a) Semmelhack, M. F.; Schmid, C. R.; Cortés, D. A.; Chou, C. S. *J. Am. Chem. Soc.* **1984**, *106*, 3374; (b) Gamez, P.; Arends, I. W. C. E., Reedijk, J.; Sheldon, R. A. *Chem. Commun.* **2003**, 2414; (c) Merbouh, N.; Bobbitt, J. M.; Brückner, Ch. *Org. Prep. Proc. Int.* **2004**, *36*, 1; (d) Bobbitt, J. M.; Brückner, C.; Merbouh, N. *Org. React*. **2009**, *74*, 103; (e) Caron, S.; Dugger, R. W.; Ruggeri, S. G.; Ragan, J. A.; Ripin, D. H. B. *Chem. Rev*. **2006**, *106*, 2943; (f) Ciriminna, R.; Pagliaro, M. *Org. Process Res. Dev.* **2010**, *14*, 245; (g) Hoover, J. M.; Stahl, S. S. *J. Am. Chem.*

Soc. **2011**, *133*, 16901; (h) Ma, S.; Liu, J.; Li, S.; Chen, B.; Cheng, J.; Kuang, J.; Liu, Y.; Wan, B.; Wang, Y.; Ye, J.; Yu, Q.; Yuan, W.; Yu, S. *Adv. Synth. Catal.* **2011**, *353*, 1005.

(4) Blanchard, P.-Y.; Niebel, C.; Boisard, S.; Alévêque, O.; Sanguinet, L.; Dias, M.; Breton, T.; Gautier, Ch.; Levillan, E. *New J. Chem.* **2012**, *36*, 546.

(5) Kavala, M.; Boča, R.; Dlháň, Ľ.; Brezová, V.; Breza, M.; Kožíšek, J.; Fronc, M.; Herich, P.; Švorc, Ľ.; Szolcsányi, P. *J. Org. Chem.* **2013**, *78*, 6558.

(6) Likhtenshtein, G.; Yamauchi, J.; Nakatsuji, S.; Smirnov, A. I.; Tamura, R.; Ed., *Nitroxides: Applications in Chemistry, Biomedicine, and Materials Science*; Wiley-VCH: Weinheim, **2008**.

(7) (a) Oyaizu, K.; Nishide, H. *Adv. Mater.* **2009**, *21*, 2339; (b) Kim, J.-K.; Ahn, J.-H.; Cheruvally, G.; Chauhan, G. S.; Choi, J.-W.; Kim, D.-S.; Ahn, H.-J.; Lee, S. H.; Song, Ch. E. *Met. Mater. Int.* **2009**, *15*, 77; (c) Koshika, K.; Chikushi, N.; Sano, N.; Oyaizu, K.; Nishide, H. *Green Chem.* **2010**, *12*, 1573; (d) Janoschka, T.; Hager, M. D.; Schubert, U. S. *Adv. Mater.* **2012**, *24,* 6397.

(8) (a) Chiarelli, R.; Novak, M. A.; Rassat, A.; Tholence, J. L. *Nature* **1993**, *363*, 147; (b) Wu, Y.; Hirai, Y.; Tsunobuchi, Y.; Tokoro, H.; Eimura, H.; Yoshio, M.; Ohkoshi, S.; Kato, T. *Chem. Sci.* **2012**, *3*, 3007.

(9) (a) Zhang, Z.; Chen, P.; Murakami, T. N.; Zakeeruddin, S. M., Grätzel, M. *Adv. Funct. Mater.* **2008**, *18*, 341; (b) Kato, F.; Hayashi, N.; Murakami, T.; Okumura, Ch.; Oyaizu, K.; Nishide, H. *Chem. Lett*. **2010**, *39*, 464; (c) Kato, F.; Kikuchi, A.; Okuyama, T.; Oyaizu, K.; Nishide, H. *Angew. Chem. Int. Ed*. **2012**, *51*, 10177; (d) Grynova, G.; Barakat, J. M.; Blinco, J. P.; Bottle, S. E.; Coote, M. L. *Chem. Eur. J.* **2012**, *18*, 7582.

(10) Schattling, P.; Jochum, F. D.; Theato, P. *Chem. Commun.* **2011**, *47*, 8859.

(11) (a) Sosnovsky; G. Lukszo, J.; Brasch, R. C.; Eriksson, U. G.; Tozer, T. N. *Eur. J. Med. Chem*. **1989**, *24*, 241; (b) Zhelev, Z.; Bakalova, R.; Aoki, I.; Matsumoto, K.; Gadjeva, V.; Anzai, K.; Kanno, I. *Chem. Commun*. **2009**, 53.

(12) (a) Hahn, S. M.; Tochner, Z.; Krishna, C. M.; Glass, J.; Wilson, L.; Samuni, A.; Sprague, M.; Venzon, D.; Glatstein, E.; Mitchell, J. B.; Russo, A. *Cancer Res.* **1992**, *52*, 1750; (b) Cotrim, A. P.; Hyodo, F.; Matsumoto, K.; Sowers, A. L.; Cook, J. A.; Baum, B. J.; Krishna, M. C.; Mitchell, J. B. *Clin. Cancer. Res.* **2007**, *13*, 4928; (c) Frantz, M.-C.; Pierce, J. G.; Pierce, J. M.; Kangying, L.; Qingwei, W.; Johnson, M.; Wipf, P. *Org. Lett*. **2011**, *13*, 2318.

(13) Metz, J. M.; Smith, D.; Mick, R.; Lustig, R.; Mitchell, J.; Cherakuri, M.; Glatstein, E.; Hahn, S. M. *Clin. Cancer. Res.* **2004**, *10*, 6411.

(14) (a) Wilcox, C. S.; Pearlman, A. *Pharmacol. Rev.* **2008**, *60*, 418; (b) Wilcox, C. S. *Pharmacol. Ther.* **2010**, *126*, 119; (c) Tan, N. P. H.; Taylor, M. K.; Bottle, S. E.; Wright, Ch. E.; Ziogas, J.; White, J. M.; Schiesser, C. H., Jani, N. V. *Chem. Commun*. **2011**, *47*, 12083.

(15) Rosen, G. M.; Schneider, E.; Shortkroff, S.; Tsai, P.; Winalski, C. S. *J. Chem. Soc., Perkin Trans. 1* **2002**, 2663.

(16) Ma, Y.; Lyons, C.; Price, P.; Chechik, V. *Org. Biomol. Chem.* **2011**, *9*, 5573.

(17) Crich, D.; Grant, D.; Bowers, A. A. *J. Am. Chem. Soc.* **2007**, *129*, 12106.

(18) Gravert, D.; Datta, A.; Wentworth Jr., P.; Janda, K. *J. Am. Chem. Soc.* **1998**, *120*, 9481.

(19) Zakrzewski, J.; Hupko, J. *Org. Prep. Proc. Int.* **2003**, *35*, 387.

(20) Pirrwitz, J.; Damerau, W. *Z. Chem.* **1976**, *16*, 401.

(21) Basel, Y.; Hassner, A. *J. Org. Chem.* **2000**, *65*, 6368.

(22) Blinco, J. P.; Hodgson, J. L.; Morrow, B. J.; Walker, J. R.; Will, G. D.; Coote, M. L.; Bottle, S. E. *J. Org. Chem.* **2008**, *73*, 6763.

(23) (a) Krishna, M. C.; Grahame, D. A.; Samuni, A.; Mitchell, J. B.; Russo, A. *Proc. Natl. Acad. Sci. U.S.A.* **1992**, *89*, 5537; (b) Baur, E. J.; Wang, S.; Brandt, M. C. *Anal. Chem.* **1996**, *68*, 3815; (c) Goldstein, S.; Samuni, A.; Hideg, K.; Merenyi, G. *J. Phys. Chem. A* ***2006****, 110*, 3679.

(24) Durand, G.; Choteau, F.; Prosak, R. A.; Rockenbauer, A., Villamena, F. A.; Puccia, B. *New J. Chem.* **2010**, *34*, 1909.

(25) Morris, S.; Sosnovsky, G.; Hui, B.; Huber, C. O.; Rao, N. U. M.; Swart, H. M. *J. Pharm. Sci.* **1991**, *80*, 149.

(26) Yamasaki, T.; Matsuoka, Y.; Mito, F.; Yamato, M.; Yamada, K. *Asian J. Org. Chem.* **2013**, *2*, 388.

(27) Isogai, T.; Saito, T.; Isogai, A. *Biomacromolecules* **2010,** *11,* 1593.

(28) Jia, M.; Tang, Y.; Lam, Y.-F.; Green, S. A.; Blough, N. V. *Anal. Chem.* **2009,** *81,* 8033.

(29) Yamasaki, T.; Mito, F.; Ito, Y.; Pandian, S.; Kinoshita, Y.; Nakano, K., Murugesan, R.; Sakai, K.; Utsumi, H.; Yamada, K. *J. Org. Chem.* **2011**, *76*, 435.

(30) (a) Rieger, P.H. *Electron Spin Resonance Analysis and Interpretation*; RSC Publishing: Cambridge UK, **2007**; (b) Ottaviani, M. F.; Modelli, A.; Zeika, O.; Jockusch, S.; Moscatelli, A.; Turro, N. J. *J. Phys. Chem. A* **2012**, *116*, 174; (c) Glarum, S. H.; Marshall, J. H. *J. Chem. Phys.* **1967**, *47*, 1374; (d) Parmon, V. N., Kokorin, A. I.; Zhidomirov, G. M. *J. Struct. Chem.* **1977**, *17*, 104; (e) Grampp, G.; Landgraf, S.; Grigorev, I. A.; Shapiro, A. B.; Kokorin, A. I. *Appl. Magn. Reson.* **2000**, *19*, 187; (f) Grampp, G.; Rasmussen, K.; Kokorin, A. I. *Appl. Magn. Reson.* **2004**, *26*, 245; (g) Kokorin, A. I. *Appl. Magn. Reson.* **2004**, *26*, 253; (h) Kokorin, A. I.; Tran, V. A.; Rasmussen, K.; Grampp, G. *Appl. Magn. Reson.* **2006**, *30*, 35.

(31) (a) Parmon, V. N.; Zhidomirov, G. M. *Mol. Phys.* **1974,** *27*, 367; (b) Parmon, V. N.; Kokorin, A. I.; Zhidomirov, G. M.; Zamaraev, K. I. *Mol. Phys.* **1975,** *30*, 695; (c) Parmon, V. N.; Zhidomirov, G. M. *Mol. Phys.* **1976,** *32*, 613.

(32) Ysacco, C.; Rizzato, E.; Virolleaud, M.-A.; Karoui, H.; Rockenbauer, A.; Le Moigne, F.; Siri, D.; Ouari, O.; Griffin, R. G.; Tordo, P. *Phys. Chem. Chem. Phys*. **2010**, *12*, 5841.

(33) (a) Komaguchi, K.; Iida, T.; Goh, Y.; Ohshita, J.; Kunai, A.; Shiotani, M. *Chem. Phys. Lett*. **2004**, *387*, 327; (b) Szydłowska, J.; Pietrasik, K.; Głaz, Ł.; Kaim, A. *Chem. Phys. Lett*. **2008**, *460*, 242; (c) Riplinger, C.; Kao, J. P. Y.; Rosen, G. M.; Kathirvelu, V.; Eaton, G. R.; Eaton, S. S.; Kutateladze, A.; Neese, F. *J. Am. Chem. Soc.* **2009**, *131*, 10092.

(34) Allen, F. R. *Acta Crystallogr.* **2002**, *B58*, 380.

(35) Bernstein, J.; Devis, R. E.; Shimoni, L.; Chang, N.-L. *Angew. Chem., Int. Ed. Engl.* **1995**, *34*, 1555.

(36) Torres, E.; Moreno-Viguri, E.; Galiano, S.; Devarapally, G.; Crawford, P. W.; Azqueta, A.; Arbillaga, L.; Varela, J.; Birriel, E.; Di Maio, R.; Cerecetto, H.; González, M.; Aldana, I.; Monge, A.; Pérez-Silanes, S. *Eur. J. Med. Chem.* **2013**, *66*, 324.

(37) (a) Vilchéze, C.; Hartman, T.; Weinrick, B.; Jacobs, W. R. *Nature Communications* **2013**, *4*, 1881; (b) Audran, G.; Brémond, P.; Franconi, J.-M.; Marque, S. R. A.; Massot, P.; Mellet, P.; Parzyb, P.; Thiaudière, E. *Org. Biomol. Chem*. **2014**, *12*, 719.

(38) Zakrzewski, J.; Krawczyk, M. *Bioorg. Med. Chem. Lett.* **2011**, *21*, 514.

(39) Tkachev, V. V.; Sen, V. D.; Atovmyan, L. O. *Bull. Acad. Sci. USSR, Div. Chem. Sci.(Engl. Transl.)* **1987**, *36*, 1696.

(40) Duling, D. R. *J. Magn. Reson.* **1994**, *104*, 105.

(http://www.niehs.nih.gov/research/resources/software/tox-pharm/tools/index.cfm)

(41) Stoll, S.; Schweiger, A. *J. Magn. Reson.* **2006**, *178*, 42. (http://www.easyspin.org)

(42) CrysAlisPro, Oxford Diffraction Ltd., Version 1.171.36.20 (2012), Abingdon, Oxford, England.

(43) Sheldrick, G. M. *Acta Cryst.* **2008**, A64, 112.

(44) Burla, M. C.; Caliandro, R.; Camalli, M.; Carrozini, B.; Cascarano, G. L.; Giacovazzo, C.; Mallamo, M.; Mazzone, A.; Polidori, G.; Spagna, R. *J. Appl. Crystallogr.* **2012**, *45*, 357.

(45) Dolomanov, O. V.; Bourhis, L. J.; Gildea, R. J.; Howard, J. A. K.; Puschmann, H. *J. Appl. Crystallogr.* **2009**, *42*, 339.

(46) Brandenburg, K.; Berndt, M. *DIAMOND*. Crystal Impact GmbH, Bonn, Germany, **1999**.

(47) Guzei, I. *Idealized Molecular Geometry Library*, University of Wisconsin-Madison, USA, **2010**.

(48) Thorn, A.; Dittrich, B.; Sheldrick, G. M. *Acta Crystallogr.* **2012**, *A68*, 448.

(49) *Methods for Dilution Antimicrobial Susceptibility Tests for Bacteria That Grow Aerobically; Approved Standard—Fifth Edition* , Vol. 26, No.2, USA, **2000**.

(50) *Reference Method for Broth Dilution Antifungal Susceptibility Testing of Yeasts; Approved Standard—Second Edition*, Vol. 22, No. 15, USA, **2002**.

(51) Dudová, B.; Hudecová, D.; Pokorný, R.; Mičková, M.; Palicová, M.; Segľa, P.; Melník, M. *Folia Microbiol.* **2002**, *47*, 225.